Malaysian Journal of Mathematical Sciences 2(2): 173-184 (2008)

Finite Element Analysis for Oil Palm Fruit Using Open-Ended Coaxial Sensor

You Kok Yeow, Zulkifly Abbas, Kamel Ariffin Mohd Atan, Nik Mohd Asri Nik Long, Jumiah Hassan and Abdul Halim Shaari
Institut Penyelidikan Matematik, Universiti Putra Malaysia, 43400 UPM Serdang, Selangor

ABSTRACT

This paper presents a new technique of predicting the reflection coefficient of a microwave sensor for oil palm fruits using finite element method (FEM). Comparison results between measured and calculated reflection coefficient were found to be in good agreement with magnitude and phase errors of less than 0.05 and 0.2 radian.

Keywords*:* Finite element method; Oil palm Fruit; Coaxial probe; Reflection coefficient

INTRODUCTION

The open-ended coaxial technique is one of the most widely used sensor to determine the dielectric properties of materials at microwave frequencies. The permittivity of the material under test is usually calculated from measured reflection coefficient, Γ using analytical admittance model (Levine *et al*., 1951 ; Marcuvitz, 1964). Unfortunately, the analytical solutions are not accurate due to the assumption of homogeneous in those formulations, such as used an approximated approach to solve the singularity point in the equations (Levine *et al*., 1951 ; Marcuvitz, 1964). Various computational techniques have been developed to solve electromagnetic (EM) related problems not amenable to analytical or exact solutions. The most common techniques include the finite element method (FEM), the method of moment (MoM) and the finite difference time domain (FDTD).

The FEM is more conformable to irregular wave problem than FDTD, since a mesh of finite difference computational is only in regular rectangular shape. In contrast, the arbitrary mesh shape of FEM can handle this problem. The main disadvantage of FEM is that the human preparation and program run time is more than FDTD. For open boundary problem, the MoM is the best choose to solve the problem, but for overall procedures, the MoM is much difficult than FEM for derivation of governing equation.

Nevertheless, the limiting factor of electromagnetic computations is the unknown count, N and the associated demands on storage and solution time. Thus, the finite element techniques which have $O(N)$ storage and solution time are necessary to tackle three-dimensional problems. This is one of the reasons for the popularity of partial differential equation techniques over integral equation approaches, such as moment of method (MoM), as the latter lead to dense matrices with $O(N^2)$.

The two-dimensional scalar finite element method (FEM) was introduced by Gajda *et al* (1983) to solve Laplace's equation indirectly in the rotationally symmetric region of air-filled open-ended coaxial line. Nevertheless, the simple Laplace's equations is neglected a space charge distribution, σ, as well as only suitable applied in region with constant permittivity (Silvester, 1994). Besides, the capacitance expression obtained from scalar FEM is only satisfied at lower frequency. The vector FEM in High Frequency Structure Simulator (HFSS) was used by Blackham *et al*. (1993) to investigate the commercial coaxial probe but restricted to reflection properties of air. In this paper, we extend the application of FEM to the determination of reflection coefficient of oil palm fruits.

Vector Finite Element Analysis of Open-Ended Coaxial Probe

Partial Difference Equation

An open-ended coaxial probe consists of inner and outer conductor, with radius a and b, respectively. The outer conductor has a flange extending to infinity as shown in Figure 1.

For any TM waves, the partial difference equation (PDE) formulation is given:

$$\vec{\nabla}\times\left(\frac{1}{\varepsilon}\vec{\nabla}\times\vec{H}\right)-k_o^2\mu\ \vec{H}=0 \tag{1}$$

where $\varepsilon=\varepsilon_o\varepsilon_r$ is the permittivity of materials.

For open coaxial line, magnetic field, $\vec{H}$ is a function of ρ and z, but independent of ϕ, thus

$$-\frac{\partial}{\partial\rho}\left(\frac{1}{\varepsilon\ \rho}\frac{\partial}{\partial\rho}\left(\rho H_\phi\right)\right)-\frac{1}{\varepsilon}\frac{\partial^2}{\partial z^2}H_\phi-\mu\ k_o^2 H_\phi=0 \tag{2}$$

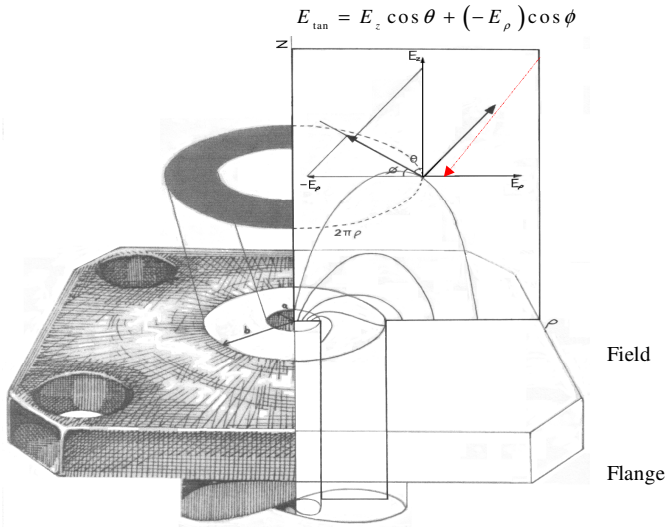

Figure 1: Coaxial line with baffle

The first order of differential arguments in (2) can be represented by electric field components (Levine *et al*., 1951):

$$-j\omega E_z=-\frac{1}{\varepsilon\ \rho}\frac{\partial}{\partial\rho}\left(\rho H_\phi\right) \tag{3}$$

$$j\omega E_\rho=-\frac{1}{\varepsilon}\frac{\partial}{\partial z}H_\phi \tag{4}$$

To avoid singularities at the axis $(\rho=0)$ of rotation, we insert a dependent variable U, defined as the angular component of the magnetic field divided by the radial space coordinate ρ

$$U=\frac{H_\phi}{\rho} \tag{5}$$

into (2) to obtain

$$-\frac{\partial}{\partial\rho}\left(\frac{\rho}{\varepsilon}\frac{\partial U}{\partial\rho}+\frac{2U}{\varepsilon}\right)-\frac{\rho}{\varepsilon}\frac{\partial^2 U}{\partial z^2}-\rho\mu\, k_o^2 U=0 \tag{6}$$

Discretization

For the k th such element, the trial function for $U^{(k)}$ can be assumed as (Sumbar *et al*., 1991; Silvester, 1994):

$$U^{(k)}=\sum_{j=1}^{N}U_j^{(k)}\alpha_j \tag{7}$$

where $U_j^{(k)}$ are the unknown complex constants, which remain to be determined. α_j are the real-valued linear interpolation functions (as a shape functions of coordinates ρ and z). N represents the number of nodes, which is defining the k th element.

Weighted Residual Techniques

The equation (7) is substituted into the governing equation (6), multiplying the result by the set of shape functions α_i and integrating over the area of the element, yields

$$\sum_{j=1}^{N}U_j^{(k)}\iint_{(k)}\left[-\frac{\partial}{\partial\rho}\left(\frac{\rho}{\varepsilon}\frac{\partial\alpha_j}{\partial\rho}+\frac{2\alpha_j}{\varepsilon}\right)-\frac{\rho}{\varepsilon}\frac{\partial^2\alpha_j}{\partial z^2}-\rho\mu\, k_o^2\alpha_j\right]\alpha_i\, d\rho dz=0 \tag{8}$$

Equation (8) can be integrated by parts to give (Sumbar *et al*., 1991)

$$\sum_{j=1}^{N}U_j^{(k)}\iint_{(k)}\left[-\alpha_i\frac{\partial}{\partial\rho}\left(\frac{\rho}{\varepsilon}\frac{\partial\alpha_j}{\partial\rho}+\frac{2\alpha_j}{\varepsilon}\right)-\alpha_i\frac{\partial}{\partial z}\left(\frac{\rho}{\varepsilon}\frac{\partial\alpha_j}{\partial z}\right)\right]d\rho dz$$
$$+\sum_{j=1}^{N}U_j^{(k)}\iint_{(k)}\left[-\left(\frac{\rho}{\varepsilon}\frac{\partial\alpha_j}{\partial\rho}+\frac{2\alpha_j}{\varepsilon}\right)\frac{\partial\alpha_i}{\partial\rho}-\left(\frac{\rho}{\varepsilon}\frac{\partial\alpha_j}{\partial z}\right)\frac{\partial\alpha_i}{\partial z}-\alpha_i\rho\mu\, k_o^2\alpha_j\right]d\rho dz=0 \tag{9}$$

The first double integral in (9) can be transformed into a contour integral by Green's theorem (Sumbar *et al*., 1991), as well as relationship of equations (3), (4), (5) and (7), thus

$$\sum_{j=1}^{N} U_j^{(k)} \iint_{(k)} \left[-\alpha_i \frac{\partial}{\partial \rho}\left(\frac{\rho}{\varepsilon}\frac{\partial \alpha_j}{\partial \rho} + \frac{2\alpha_j}{\varepsilon} \right) - \alpha_i \frac{\partial}{\partial z}\left(\frac{\rho}{\varepsilon}\frac{\partial \alpha_j}{\partial z} \right) \right] d\rho dz$$
$$= -\oint_{(k)} \left[\left(j\omega E_\rho^{(k)} \right)\cos\phi^{(k)} + \left(-j\omega E_z^{(k)} \right)\cos\theta^{(k)} \right] \alpha_i d\ell$$
$$= -\oint_{(k)} j\omega E_{\tan}^{(k)} \alpha_i d\ell \qquad (10)$$

Where ℓ is the path of integration follows the perimeter of the *k*th element in a counterclockwise direction and

$$j\omega E_\rho^{(k)} \approx -\sum_{j=1}^{N} U_j^{(k)} \frac{\rho}{\varepsilon}\frac{\partial \alpha_j}{\partial z} \qquad (11)$$

$$-j\omega E_z^{(k)} \approx -\sum_{j=1}^{N} U_j^{(k)} \left(\frac{\rho}{\varepsilon}\frac{\partial \alpha_j}{\partial \rho} + \frac{2}{\varepsilon}\alpha_j \right) \qquad (12)$$

Therefore, (9) become

$$\sum_{j=1}^{N} U_j^{(k)} \iint_{(k)} \left[-\left(\frac{\rho}{\varepsilon}\frac{\partial \alpha_j}{\partial \rho} + \frac{2\alpha_j}{\varepsilon} \right)\frac{\partial \alpha_i}{\partial \rho} - \left(\frac{\rho}{\varepsilon}\frac{\partial \alpha_j}{\partial z} \right)\frac{\partial \alpha_i}{\partial z} - \alpha_i \rho \mu_r k_o^2 \alpha_j \right] d\rho dz$$
$$= \oint_{(k)} j\omega E_{\tan}^{(k)} \alpha_i d\ell \qquad (13)$$

The fields were integrated to get an average for the whole cylindrical boundary, thus the field has to be multiplied by a factor $2\pi\rho$ while integrating. Finally, **t**he Galerkin's principle for nodal finite elements is implemented in FEM for transformation of the equation (13) to equivalent systems of algebraic equations

$$[S][U] = [f] \qquad (14)$$

Where $[S]$ is the coefficient matrix of global system on the left-hand side of equation (13). $[U]$ is the solution vector matrix of undetermined

coefficients at the nodes, which representing the values of $\left(\approx H_\phi / \rho\right)$. $\left[f\right]$ is the vector matrix of contour integrals on the right-hand side of equation (13).

Boundary Conditions

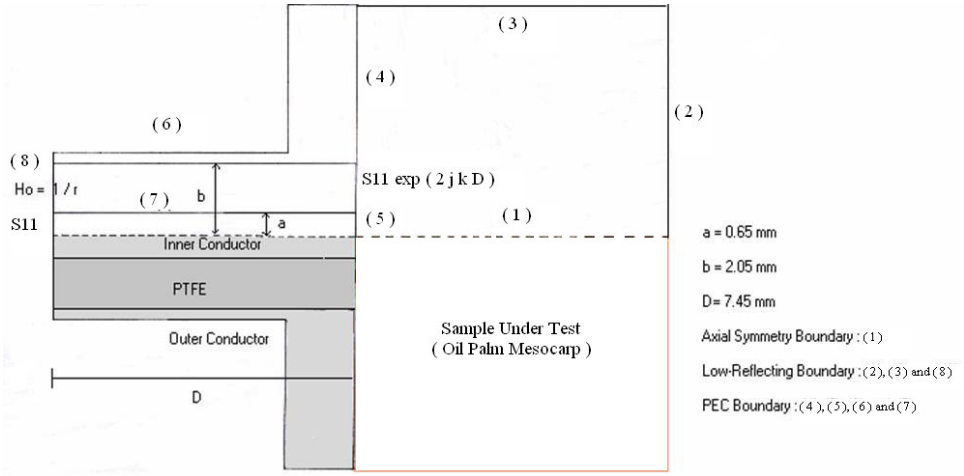

Figure 2: Rotationally symmetric region of open-ended coaxial line.

The field in coaxial line is assumed to be a TEM wave,

$$H_\phi = \frac{1}{\rho} e^{-jk_o z} \tag{15}$$

Equations (15) is applied to the excitation boundary (8) of the coaxial line with the phase factor, $e^{-jk_o z}$ is assumed equal to 1 as shown in Figure 2. The open-ended coaxial probe has an inner radius, a = 0.65 mm and an outer radius, b = 2.05 mm of the outer conductor. The inner of the coaxial line is made of PTFE or Teflon ($\varepsilon_r = 2.05$), while the outer medium of the coaxial probe is air ($\varepsilon_r = 1$) or lossy medium.

All conductors of coaxial probe are assumed perfect. Consequently, the continuity boundary conditions for tangential component of the electric field are applied at a border of conductors.

$$\hat{n} \times \vec{E} = 0 \tag{16}$$

At outer boundary, the continuity boundary condition (Perfect Electric Conducting (PEC)) sets the tangential component of the electric field, E_z to zero. The term low-reflecting means that only a small part of the wave is reflected. The wave propagates through the boundary almost as if it was not present. Generally, the low reflecting or called radiation boundary is based on the difference between the total field and the field of the incident wave (Webb *et al*., 1995):

$$\vec{H}_t = P(\vec{E}) + \vec{H}_t^{inc} - P\left(\vec{E}^{inc}\right) \tag{17}$$

where superscript *inc* denotes the incident field and *P* is a function of the electric field over the surface. For coaxial antenna or radiator, the relation ship between $\vec{H}$ and $\vec{E}$ at scatter region is expressed as (Sumbar *et al*., 1991):

$$\vec{H} = \frac{\hat{e}_z \times \vec{E}}{\eta} \tag{18}$$

The unit vector $\hat{e}_z$ points in the direction of propagation, which is radial outward from the center of the antenna. While η is the complex intrinsic impedance of the medium

$$\eta = \sqrt{\frac{\mathrm{j}\omega\mu}{\sigma + \mathrm{j}\omega\varepsilon}} \tag{19}$$

By aid of (19), hence (18) become (The MathWorks, Inc, 2002):

$$\hat{e}_z \times \sqrt{\varepsilon}\vec{E} = -2\sqrt{\mu}H_{oz} + \sqrt{\mu}H_z \tag{20a}$$

$$\approx -\sqrt{\mu}H_\phi \tag{20b}$$

where $E_{\tan} = \hat{e}_z \times \vec{E}$ and $\sigma = 0$. Substituting (5) into (20b), yields

$$E_{\tan} = -\left(\sqrt{\mu/\varepsilon}\right)\rho\frac{H_\phi}{\rho} \tag{21a}$$

$$= -\left(\sqrt{\mu/\varepsilon}\right)\rho U \tag{21b}$$

Subsequently, the trial solution (7) is substituted for U and the integral on right-hand side of (13) is written as:

$$\oint_{(k)} E_{\tan}^{(k)}\alpha_i dl = -\oint_{(k)}\left[\left(\sqrt{\mu/\varepsilon}\right)^{(k)}\sum_{j=1}^{N}U_j^{(k)}\alpha_j\right]\alpha_i dl \tag{22a}$$

$$= -\sum_{j=1}^{N}U_j^{(k)}\oint_{(k)}\alpha_j\left[\left(\sqrt{\mu/\varepsilon}\right)^{(k)}\right]\alpha_i dl \tag{22b}$$

The axial symmetry boundary condition is along the z-axis. At the symmetry axis, the tangential part of the magnetic may vanish and the meridional fields must satisfy the conditions

$$E_\rho = 0 \tag{23a}$$

$$\frac{\partial E_z}{\partial \rho} = 0 \tag{23b}$$

Final Interpretation

The magnetic field, H_ϕ at each radius points on excitation boundary (z = 0) can be written in terms of reflection coefficient, Γ:

$$H_\phi = H_{\phi\_in}\left(1-\Gamma\right) \tag{24a}$$

$$= \frac{1}{\rho}\left(1-\Gamma\right) \tag{24b}$$

where H_{ϕ_in} is the incident magnetic field on the excitation boundary. From (24), the reflection coefficient, Γ (or S_{11}) can be deduced as

$$\Gamma = \frac{H_{\phi\_in} - H_{\phi}}{H_{\phi\_in}} \tag{25}$$

The aperture reflection coefficient, Γ_A at $z = D$ plane (aperture probe) with respect to Γ at $z = 0$ (excitation plane) is defined as

$$\Gamma_A = \Gamma e^{2jk_c D} \tag{26}$$

where k_c is the propagation constant of the coaxial probe. D is equal to 7.45 mm.

RESULTS

Our study is based on both FEM simulations and experimental measurements, as well as compare to quasi-static approach (Levine *et al*., 1951 ; Marcuvitz, 1964).. The dispersive properties of the water present in the fruit were obtained from Cole-Cole model found in the literature (Nyshadham *et al*., 1992). The finite element mesh consists more than 5000 arbitrary triangular elements (double-refine mesh). Figure 3 (a) and 3 (b) show that the comparison between reflection coefficient of the fruits predicted by FEM and measured data using HP8720B vector network analyzer (VNA).

The variation in the magnitude, $|\Gamma|$ and phase, ϕ of the reflection coefficient with moisture content, *m.c* for different frequencies are shown respectively in Figure 3 (a) and (b). The measured magnitude, $|\Gamma|$ and phase, ϕ are in good agreement with FEM simulations results. The relative complex permittivity, ε_r^* used in simulations is obtained from measurements using commercial HP 85070B probe. The figures suggested ϕ vary linearly with the amount of moisture content in the oil palm mesocarp, but not for $|\Gamma|$, since $|\Gamma|$ illustrates a quadratic plotted shape with respect to moisture content, *m.c* at frequency up to 3 GHz. Besides that, the measured data of $|\Gamma|$ are less precise than phase, ϕ. It is also observed that the data for $|\Gamma|$ is less sensitive to moisture content up to 5 GHz. Obviously, magnitude of reflection coefficient, $|\Gamma|$ is not quite suitable to monitor fruit ripeness based on bandwidth measurements. In contrast, the sensitivity in ϕ with respect to moisture content, *m.c* is quite constant for all the frequencies. Therefore, it is suggested that the phase of reflection coefficient, ϕ is most flexible parameter to relate the moisture content, *m.c* of mesocarp.

The measurements for variations in magnitude and phase of complex reflection coefficient, Γ_{Actual} with thickness fruit sample for 4 GHz are illustrated in Figure 4. In this work, it is harder to obtain good controlled environment, especially the non-uniform cutting of sample, as well as orientation fiber of fruit sample. Nevertheless, the finite element method simulation values are available in Figure 4 as reference. As our knowledge, a characterized of materials using microwave technique basically more influence by phase parameters than magnitude. The numerical results revealed that the phase of reflection coefficient is assumed to be constant as long as the thickness sample is exceeded 2.5 mm. The phase of reflection coefficient, ϕ is slightly increasing after 2.5 mm, because of an uncertainty in numerical modeling. The uncertainty is mainly caused by the constant number of mesh in simulation area, since the modeling area (thickness sample) is increasing.

Simulations Performance

The program runtime is mainly depended on the number of refined mesh, as well as computer resources. It should be noted that graphical programming would not have been feasible without the recent advances in processing speed and memory capacity. As example, for free space sample with dimension 6 × 6 cm (axial × transverse), the runtime and reflection coefficient results are based on the number of mesh as tabulated in Table 2. The simulation was implemented using FEMLAB (The MathWorks, Inc, 2002) on a PC with a 1.6 GHz Pentium 4 processor, 376 MB SDRAM and 6 GB free disk space.

TABLE 2 The runtime and reflection coefficient of free space are based on the number of mesh.

Nodes	Elements	Time (rad)	$\|\Gamma\|$	ϕ
403	725	~ 6 s	0.96138	-
		0.038205		
1530	2900			
		~10 s	0.99699	-
5959		0.071578		
11600				
23517		~36 s	0.99976	-
46400		0.074425		
		~15 min	0.99996	-
		0.074782		

CONCLUSIONS

In this work, a vector finite element method is used to solve the wave equation in the two dimension rotationally symmetric region of open-ended coaxial sensor for determination of reflection coefficient of oil palm fruits. The results were close in agreement with measured data found using vector network analyzer.

REFERENCES

A. Nyshadham, C. L. Sibbald, and S. S. Stuchly, 1992. Permittivity measurements using open-ended sensors and reference liquid calibration – An uncertainty analysis, *IEEE Trans. Microwave Theory Tech*, **40**, pp. 305-314

A. Wexler, 1969.Computation of electromagnetic fields", *IEEE Trans. Microwave Theory Tech,* **17**, pp. 416-439

D. V. Blackham, and R. D. Pollard, 1993.Finite element analysis of open-ended coaxial lines", *Microware Symposium Digest, IEEE International*. **5**, pp. 1247-1240,

E. Sumbar, F. E. Vermeulen, and F. S. Chute, 1991. Implementation of radiation boundary conditions in the Finite Element Analysis of

Electromagnetic wave propagation, *IEEE Trans. Microwave Theory and Technique*, **39**, pp. 267-273

G. B.Gajda, and S. S. Stuchly, 1983.Numerical analysis of open-ended coaxial lines", *IEEE Trans. Microwave Theory Tech*, **31,** pp. 380-384,

H. Levine, and C. H. Papas, 1951.Theory of the circular diffraction antenna, *J. Appl. Phy*, **22**(1), pp. 29-43

J. G. Maloney, G. S. Smith, and JR. W. R. Scott, 1990. Accurate computation of the radiation from simple antennas using the finite-difference time-domain method, *IEEE Trans. Antennas Propagation,* **38**, pp. 1059-1068,

J. P. Grant, R. N. Clarke, G. T. Symm and N. M. Spyrou, 1989. A critical study of the open-ended coaxial line sensor technique for RF and microwave complex permittivity measurements", *J. Phys. E: Sci. Instrum*, **22**, pp. 757-770

Jr. R. C. Booton, 1992.Computational methods for electromagnetics and microwaves, New York: John Wiley & Sons

M. N. O. Sadiku, and A. K. R. Jong, 1990. A comparison of numerical methods for computing electromagnetic fields, *Proc. IEEE Southeastcon*, pp. 42-47,

M. N. O. Sadiku, 1992. *Numerical techniques in electromagnetics*, London: CRC Press

N. Marcuvitz, 1964.*Waveguide handbook*, Boston: Boston Technical Publishers

P. De Langhe, L. Martens, and D. De Zutter, 1994.Design rules for an experimental setup using an open ended coaxial probe based on theoretical modeling, *IEEE Trans. Instrum. Mea,* **43**, pp. 810-817,

P. P. Silvester, and R. L. Ferrari, 1994. *Finite elements for electrical engineers*, England: Cambridge University Press,

The MathWorks, Inc, 2002. FEMLAB Electromagnetic Module, version 2.3. Sweden: Comsol AB